Available online at www.sciencedirect.com
ScienceDirect
Polymer 48 (2007) 4547–4557
polymer
www.elsevier.com/locate/polymer

Solid-state characterization of polyethylene reactor powders and their structural changes upon annealing

Hiroki Uehara [a,*], Ayako Uehara [a], Masaki Kakiage [a], Hiroshi Takahashi [b], Syozo Murakami [c], Takeshi Yamanobe [a], Tadashi Komoto [a]

[a] Department of Chemistry, Gunma University, Kiryu, Gunma 376-8515, Japan
[b] Department of Physics, Gunma University, Maebashi, Gunma 371-8510, Japan
[c] Department of Human Environment Design, Heian Jogakuin University, Takatsuki, Osaka 569-1092, Japan

Received 7 March 2007; received in revised form 17 May 2007; accepted 18 May 2007
Available online 2 June 2007

Abstract

Polyethylene reactor powders prepared under different conditions were characterized using transmission electron microscopy, ^{1}H nuclear magnetic resonance and X-ray diffraction techniques. The molecular weight of the polyethylene reactor powders was around 1×10^5. A unique domain morphology, quite different from the usual melt- or solution-crystallized lamellar structure, was observed, independent of polymerization temperature (T_{poly}). Annealing of reactor powders caused the aggregation of these crystalline domains, due to the significant molecular motion of the amorphous chains, before melting. The critical temperature was 20 °C higher than each T_{poly}, and corresponded to the temperature at the active catalyst site producing the chain growth. The morphologies of powders prepared at the lower T_{poly} contained smaller crystals that exhibited a constrained monoclinic form. In contrast, only usual orthorhombic crystals of larger size were found within the powder prepared at the higher T_{poly}. These results suggest that the competitive processes of chain propagation and crystal growth upon polymerization may lead to unique variations of the crystalline and amorphous phases, but with similar intermediate components in the phase that connects them.

Keywords: Polyethylene; Reactor powder; ^{1}H NMR

1. Introduction

The as-polymerized reactor powder structure has been investigated especially for semi-crystalline polymers. One motivation for such investigations lies in the scientific interest concerning structural formation during polymerization. Polymerization of polyolefins and fluoro-polymers is usually performed at a temperature much lower than their usual melt-recrystallization temperature, and the resulting chain segments crystallize one another. Polyethylene (PE) has the highest crystallization rate among the polymeric materials, and its crystallization starts before the chain growth is completed. The resultant structure of the PE reactor powder has a non-equilibrium state, which is not achieved under typical crystallization conditions [1–18]. It is quite different from the conventional spherulite morphology formed through melt-recrystallization or single crystal stacking prepared by solution crystallization, where all the mature polymer chains participate in the structural formation. A detailed investigation of the reactor powder morphology may provide us information about the characteristic crystallization mechanism during polymerization.

Another motivation lies in the effective application of its less entangled state. This mainly relates to industrial interests in direct film processing from reactor powder [19,20]. The immediate crystallization with chain growth prevents the entanglement formation even under polymerization conditions producing a higher molecular weight. This unique structure

* Corresponding author. Tel.: +81 277 30 1332; fax: +81 277 30 1333.
E-mail address: uehara@chem-bio.gunma-u.ac.jp (H. Uehara).

0032-3861/$ - see front matter © 2007 Elsevier Ltd. All rights reserved.
doi:10.1016/j.polymer.2007.05.064

of the reactor powder is very advantageous for ultra-drawing processing, resulting in high-performance PE materials [12,21–25]. Similar preparations of high-performance materials from the reactor powder state are also possible for polypropylene [26] and polytetrafluoroethylene [27,28]. The resultant mechanical properties approach 70% of the theoretical values. For effective manufacturing of high-performance materials from the reactor powder, the processing temperature is often restricted below the melting temperature in order to retain the less entangled state. Therefore, better adhesion between the powder particles is a key for the resultant high performance. Powder adhesion is sometimes improved by a pre-annealing procedure before calendar rolling into the film [19].

One of the notable characteristics of the reactor powder structure is the presence of an intermediate phase included with the conventional crystalline and amorphous phases. The higher ductility of PE reactor powders suggested the coexistence of less entangled amorphous phases [12,13,16] locating between the crystalline and amorphous phases. Therefore, this intermediate phase is defined as the linker component that ties the former two phases for the reactor powder morphology. The non-equilibrium crystallization during polymerization, as mentioned above, could be the source of such intermediate structures in the reactor powder state. These different phases were characterized using a solid-state nuclear magnetic resonance (NMR) technique [13,16]. An advantage of solid-state NMR measurements is their simultaneous detection of different phases as distinguished by the characteritic molecular motion [29–45]. A combination with the morphological observations obtained by transmission electron microscopy (TEM) demonstrates the apparent relationship between structures and molecular motions for as-polymerized morphologies. In this study, the morphological and molecular motion changes upon annealing of PE reactor powder were compared using these TEM observations and solid-state ^{1}H NMR measurements. These results were used to predict the phase development mechanism during polymerization.

2. Experimental section

2.1. Samples preparation

Two polyethylene reactor powders were prepared by slurry-polymerization at $T_{poly} = 20$ °C and 70 °C in heptane with the same Ziegler catalyst system. Both polymers had a weight average molecular weight of $\sim 1 \times 10^5$ and a similar particle size around 100 μ. The sample densities were 0.94 g/cm^3 for $T_{poly} = 20$ °C powder and 0.96 g/cm^3 for $T_{poly} = 70$ °C powder. These reactor powders were placed in a glass tube, and the air was removed. A purging N_2 gas was introduced, and the tube was sealed. These sealed sample tubes were isothermally annealed for 30 min in a silicone oil bath maintained at temperatures (T_a) ranging from 40 to 160 °C. After this annealing procedure, the sample tube was removed from the oil bath and cooled under atmospheric conditions.

2.2. Measurements

TEM images were produced using a JEOL 1200EMX electron microscope operated at 80 kV. The powder samples were usually stained with RuO_4 vapor at 60 °C. The samples annealed below 50 °C, including the original reactor powders, were stained with $RuC1_3$ vapor at room temperature to eliminate the annealing effect during sample preparation. These stained powder samples were embedded in epoxy resin. The assembly was cut into thin sections 60 nm thick, using a Reichert UltraCut S. microtome.

In-situ NMR measurements during annealing of reactor powders were preformed using a JEOL MU-25 solid-state pulse NMR spectrometer equipped with a 25 MHz magnetic field. The free induction decay (FID) profile was recorded using the solid-echo method. The data were collected every 0.2 μs. Dead time before signal sampling was 2 μs. The measurement temperature was raised from room temperature up to the sample's melting temperature. Before signal sampling, the sample temperature was held isothermally for 5 min to achieve the homogeneous temperature distribution with a sample probe. Sample powder was placed in a glass tube with 7 mm diameter.

Conventional wide-angle X-ray diffraction (WAXD) patterns were recorded using a RAD-IIIA X-ray generator (Rigaku, Japan) with monochromized Cu Kα radiation at room temperature. The sample powder was mounted on a standard glass holder. The crystallite size of the powder was determined from the half-width of the reflection peak by employing the Scherrer equation assuming that there was no disorder in the arrangement of the lattice planes [46]. *In-situ* WAXD measurements during annealing of reactor powders were also performed with synchrotron radiation at station BL9C of the Photon Factory at the High-Energy Accelerator Research Organization (KEK), Tsukuba, Japan. The wavelength of the synchrotron beam was 1.50 Å. A 1 mm diameter glass tube of the sample powder was placed in a heating chamber set at the beam line. WAXD profiles were continuously recorded with a 29 s exposure time for each pattern and a 1 s time interval. A position sensitive proportional counter (PSPC) (Rigaku, PSPC-10) was used to detect diffraction intensity. The diffraction angle was represented by the PSPC detector's raw pixel corresponding to 2θ ranging from 17° to 27°. The heating rate was around 2 °C/min.

3. Results and discussion

3.1. Morphological change during annealing

The PE reactor powders used in this study were prepared at different T_{poly}s but with the same catalyst system and similar resultant MW. Fig. 1 presents the TEM images for the series of $T_{poly} = 70$ °C powders annealed at a T_a ranging from 80 °C to 130 °C, which is higher than the preparation T_{poly}. At $T_a = 80$ °C (Fig. 1a), the typical lamellar morphology of a melt- or solution-crystallized sample does not appear. Rather,

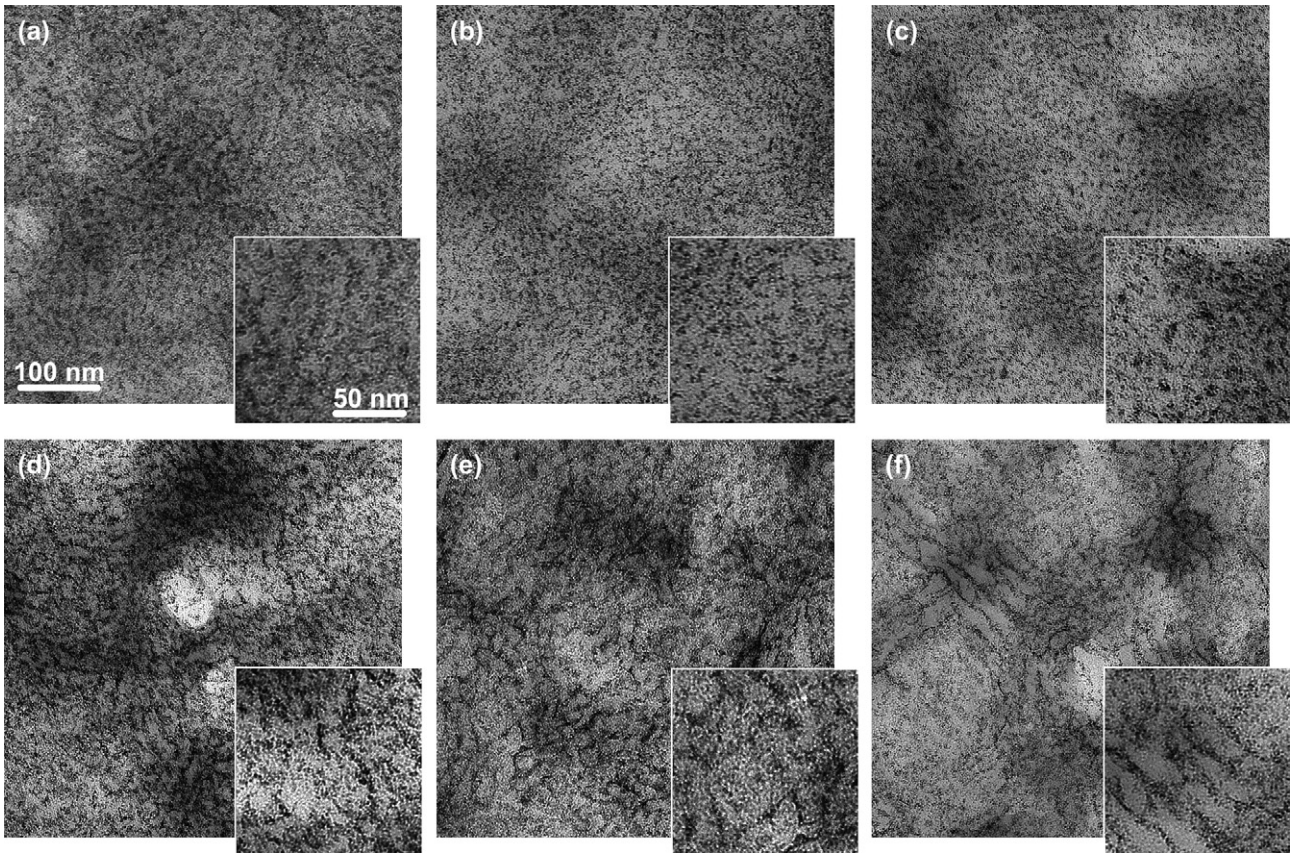

Fig. 1. TEM images of $T_{poly} = 70$ °C powder annealed at T_as (a) 80 °C, (b) 90 °C, (c) 100 °C, (d) 110 °C, (e) 120 °C, and (f) 130 °C. Enlarged images are attached at bottom right.

crystalline domains 15 nm in size are distributed throughout the powder. The image of the un-annealed sample stained at room temperature exhibits the morphology similar to that in Fig. 1a. Even the increase in T_a to 90 °C does not generate any significant change. However, at $T_a = 100$ °C and greater, the morphological change is gradually revealed. The image contrast in Fig. 1c becomes striking, due to increases of the brightness for the crystalline regions and darkness for the amorphous region. This means that the crystalline and amorphous phases were aggregated. As T_a continues to increase, the phase aggregation is further accelerated, resulting in the gradual increase in the crystalline domain size. T_as beyond 120 °C produces the lamellar structure, which is formed through melting by annealing and subsequent re-crystallization during cooling, as discussed later.

The annealing effect on the resultant morphology was also examined for the $T_{poly} = 20$ °C powder samples. Figs. 2 and 3 compare the morphologies obtained when powder annealing was performed at the higher T_a range from 80 °C to 130 °C and the lower T_a range from 40 °C to 70 °C. Fig. 3 also includes the morphology of the un-annealed $T_{poly} = 20$ °C powder. As seen in Fig. 2, the lamellar formation begins at T_as exceeding 110 °C, which is a little lower than the corresponding T_a of 120 °C for the $T_{poly} = 70$ °C powder. The WAXD data recorded while these reactor powders were heated suggest a lower melting point for the $T_{poly} = 20$ °C powder than for the $T_{poly} = 70$ °C powder, as discussed later. This difference in the lamellar-forming T_a is attributed to the smaller size of initial crystalline domains within the un-annealed $T_{poly} = 20$ °C powders displayed in Fig. 3. However, the phase arrangements were quite similar for both powder morphologies, exhibiting a homogeneous distribution of the crystalline domains. It is reasonable to conclude that this morphology is one of the universal characteristics of the PE reactor powders, independent of T_{poly}, at least in this study. The boundaries between the crystalline and amorphous phases become clear as T_a increases, especially when T_a exceeds 40 °C, and the crystalline domains begin to aggregate into the larger size. These morphological transformations are quite similar to those observed for the corresponding T_a of 90 °C for the former $T_{poly} = 70$ °C powder. No structural change is detectable below these critical T_as, so they are ascribed to the maximum temperatures to which each reactor powder was exposed during the polymerization process. Since both of these critical T_as are 20 °C higher than that of the preparation T_{poly}s, the domain-aggregating T_as correspond to the temperature near the active sites on the catalyst surface where the chain growth is progressive.

3.2. Crystalline transformation

Crystalline modification of the reactor powder is significantly affected by the preparation T_{poly} [12]. WAXD profiles

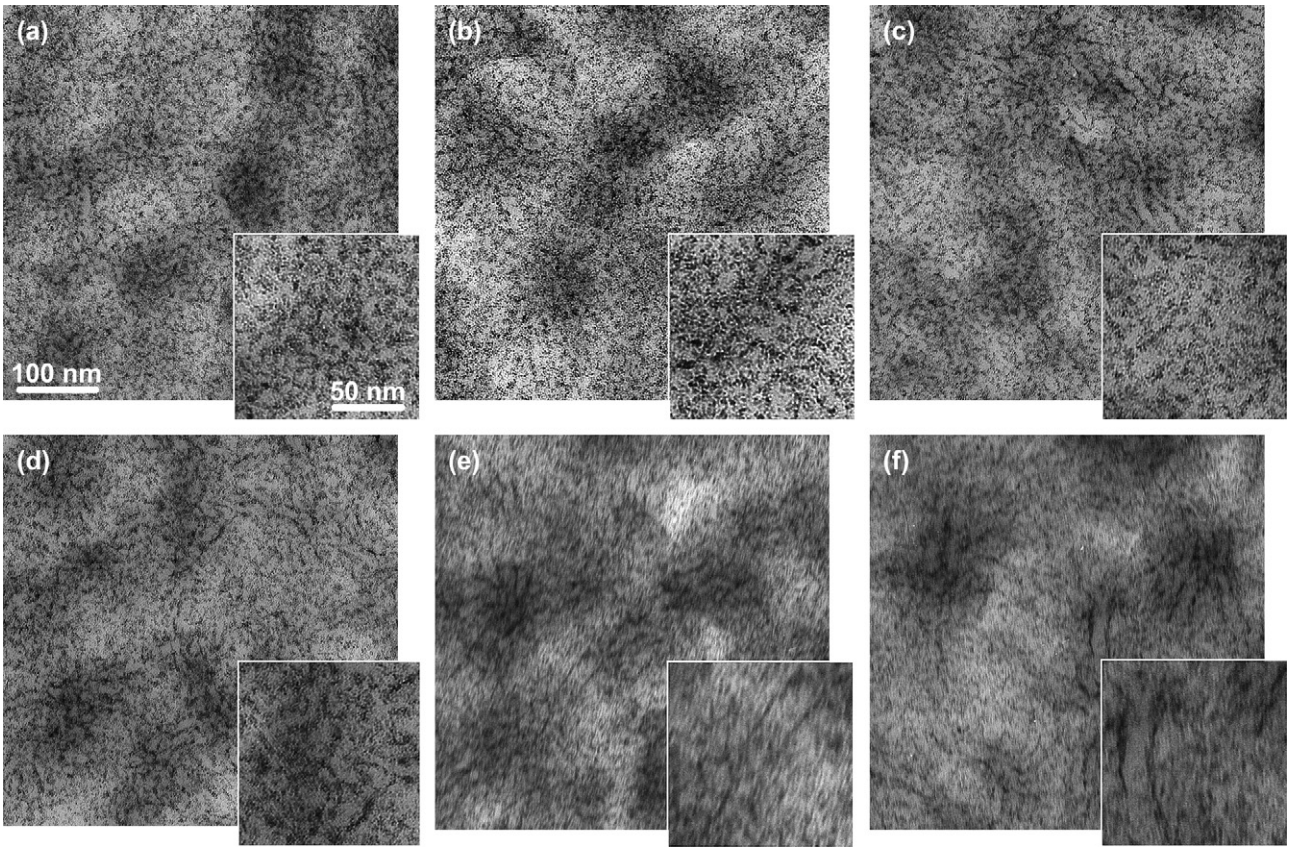

Fig. 2. TEM images of $T_{poly} = 20$ °C powder annealed at T_as (a) 80 °C, (b) 90 °C, (c) 100 °C, (d) 110 °C, (e) 120 °C, and (f) 130 °C. Enlarged images are attached at bottom right.

of the reactor powders examined in this study were recorded using a conventional X-ray facility. Fig. 4 compares the WAXD profiles for the un-annealed powders. Only peaks of (110) and (200) reflections assigned to the usual orthorhombic form are observed in the $T_{poly} = 70$ °C powder. In contrast, the $T_{poly} = 20$ °C powder exhibits the additional (010), (200) and (210) reflection peaks. These latter sets of reflections are ascribed to the constrained monoclinic form [47], which is often obtained within PEs drawn or compressed at lower temperatures [48,49]. A recent study [12] revealed that PE reactor powders also contain this monoclinic form at polymerization below 60 °C. The peak separation procedure was applied to the WAXD profiles and provided component ratios of the amorphous, monoclinic and orthorhombic crystalline phases. An analysis of the results suggests that the monoclinic form accounts for half of the crystalline phase portion within the $T_{poly} = 20$ °C powder. The crystallinity of the $T_{poly} = 20$ °C powder, calculated from the sum of these crystalline portions, is 65%, while the $T_{poly} = 70$ °C powder exhibits a crystallinity of 75%. The crystalline sizes estimated from the widths of the reflection peaks are 10 nm for the orthorhombic form and 5 nm for the monoclinic form in the $T_{poly} = 20$ °C powder. These are smaller than the 17 nm sizes for the orthorhombic form within the $T_{poly} = 70$ °C powder and coincident with the morphological features in TEM images, where the $T_{poly} = 20$ °C powder exhibits a smaller domain size.

These different crystalline forms transform during annealing. Fig. 5 compares the changes in the series of *in-situ* WAXD profiles obtained during heating the $T_{poly} = 20$ °C and $T_{poly} = 70$ °C powders. The reflection intensities are represented by a color gradation with blue as the lowest, then green, yellow, red, and white, the highest. For the $T_{poly} = 20$ °C powder, the intensity of the initial monoclinic (010) reflection is maintained until 60 °C but begins to decrease beyond 70 °C. The simultaneous growths of the orthorhombic (110) and (200) reflections are synchronized with the reduction in the monoclinic reflection intensity. At 100 °C, the monoclinic reflection almost disappears. These features suggest that the transformation from the monoclinic to the orthorhombic form is completed in the temperature range from 70 °C to 100 °C. In contrast, the orthorhombic (110) and (200) reflections in the $T_{poly} = 70$ °C powder decrease in intensity during the initial stage of annealing below 80 °C. However, their reflection intensities increase at temperatures above 90 °C. Similar initial decreases and subsequent increases of the reflection intensities were confirmed when the sum of the crystalline intensities for both the monoclinic and orthorhombic reflections was traced as a function of temperature for the $T_{poly} = 20$ °C powder. The critical temperature, where the total crystalline intensity was minimized, was 80 °C, independent of the powders. Such phenomena are closely related to the crystallinity change during heating, which will be discussed later.

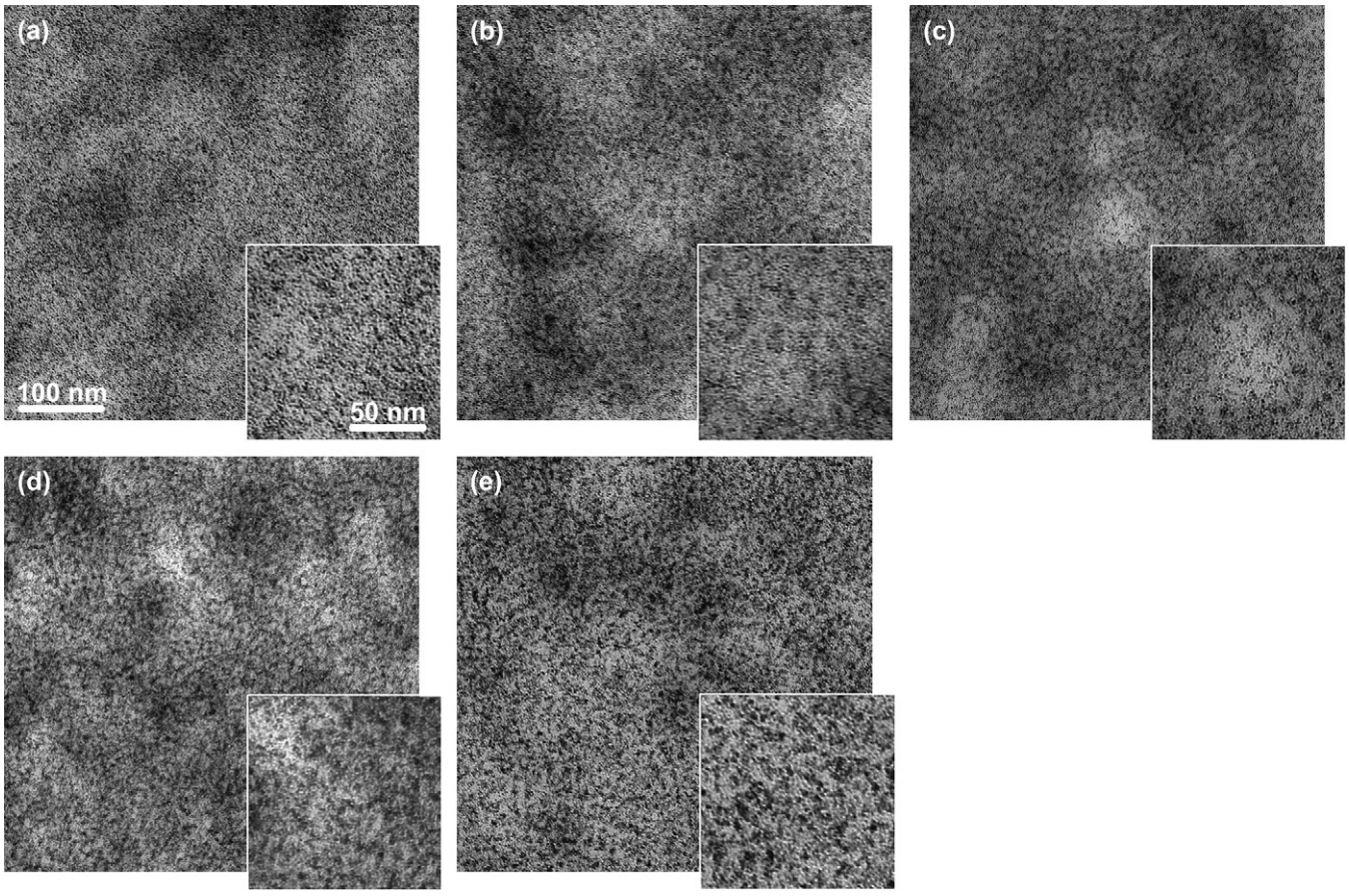

Fig. 3. TEM images of $T_{poly} = 20\ ^{\circ}C$ powder (a) un-annealed and annealed at the lower T_as of (b) 40 °C, (c) 50 °C, (d) 60 °C, and (e) 70 °C. Enlarged images are attached at bottom right.

3.3. Relaxation characteristics of different phases

The reactor powder structures were also characterized by solid-state ^1H NMR measurements. The solid-echo technique was applied in this study. Fig. 6 compares the FID profiles recorded at room temperature for the $T_{poly} = 20\ ^{\circ}C$ and $T_{poly} = 70\ ^{\circ}C$ powders. The component at the shorter time scale corresponds to the rigid component, i.e. the crystalline phase. The longer time scale corresponds to the soft component, i.e. the amorphous phase. The plots in the intermediate time region ranging from 30 to 50 μs are the same in both FID profiles, but the regions in the shorter and longer time scales exhibit a higher intensity for the $T_{poly} = 20\ ^{\circ}C$ powder than for the $T_{poly} = 70\ ^{\circ}C$ one.

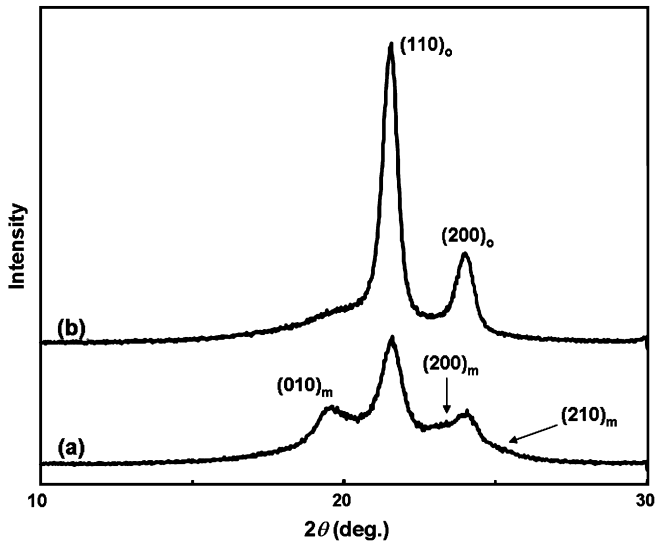

Fig. 4. WAXD patterns for the original powders prepared at $T_{poly} = (a)\ 20\ ^{\circ}C$ and (b) 70 °C. Measurement was taken at room temperature. The subscripts "o" and "m" indicate the crystal modifications of orthorhombic and monoclinic of PE.

Profile resolution was performed, assuming three relaxation components corresponding to the shorter, intermediate and longer time regions. The Weibull/Sine function [16] is known to successfully handle this type of three-component FID resolution of various PE samples crystallized under different conditions. A remarkable advantage of this function lies in its universality. It includes all of the typical relaxation functions of the Gauss/Sine equation [50] for the crystalline phase, the Weibull equation [33,51] for the intermediate phase, and the Lorentz equation for the amorphous phase, which is the most popular for NMR spectrum analysis. The intermediate Weibull equation covers the typical Gauss function. Resolution of the observed FID profile provides evaluations of the molecular motions for different phases. Fig. 7 depicts the three-component resolution results for both reactor powders. High fitting reliabilities could be confirmed from these data.

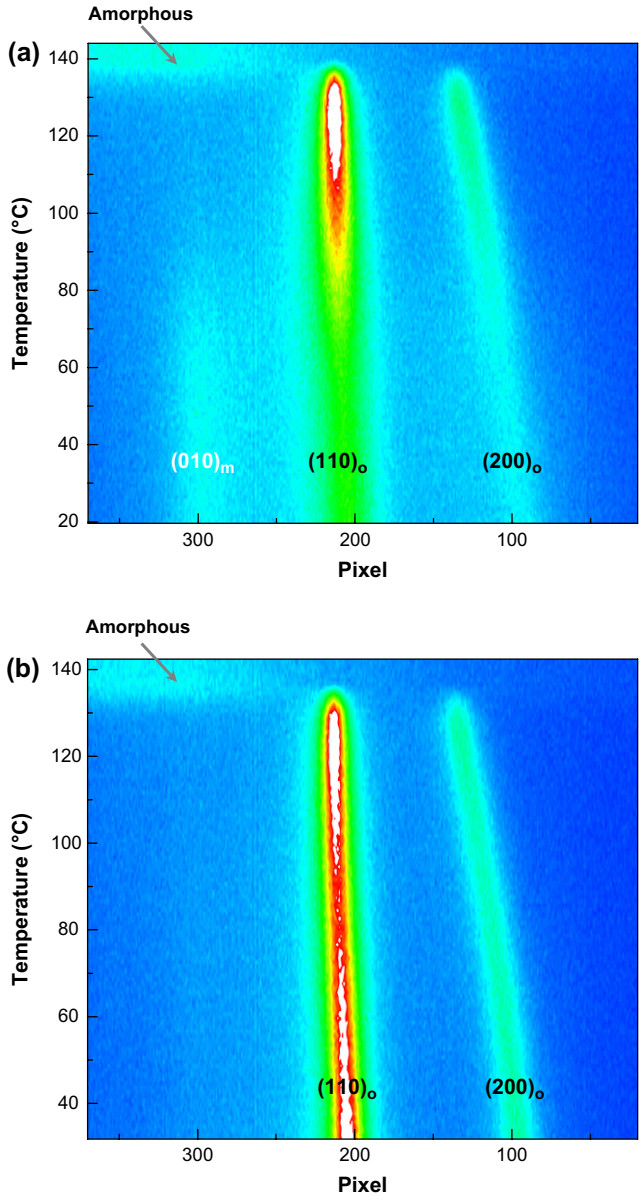

Fig. 5. Changes in WAXD patterns during heating for the powders prepared at $T_{poly} = 20$ °C (a) and 70 °C (b). The WAXD profiles obtained every 1 °C were duplicated with color gradation indicating intensity from the lowest (blue) to the highest (white). The lateral axis is represented by the raw pixel in PSPC detector, corresponding to 2θ ranging from 17° to 27°. The typical (110) and (200) reflections of usual orthorhombic form and (010) reflection of constrained monoclinic form are denoted.

Each component profile obtained from this three-phase resolution method was Fourier-transformed into a broad-line spectrum with the frequency scale, and its integral peak width (the length of the horizontal line that equally divides the total area of the peak) was then estimated [13,16]. Here, the spin-spin relaxation time, T_2, was defined as the reciprocal of the estimated integral width. The obtained T_2 values for these three phases are summarized in Table 1. Similar T_2 values were obtained for the intermediate phase, independent of T_{poly}, while those of the crystalline and amorphous phases exhibit large differences. Namely, the lower value of the crystalline

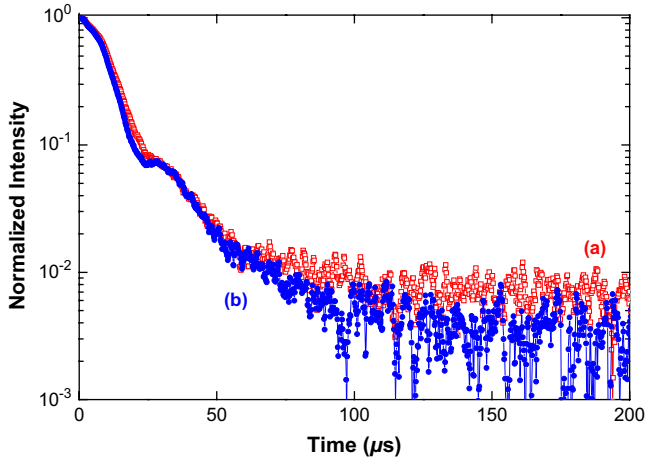

Fig. 6. Comparison of ^{1}H NMR FIDs observed at room temperature for the original powders prepared at $T_{poly} = 20$ °C (a) and 70 °C (b).

T_2 was obtained for the $T_{poly} = 70$ °C powder, but the lower value of the amorphous T_2 was evaluated for the $T_{poly} = 20$ °C powder. These results suggest that the crystalline phase is more rigid for the $T_{poly} = 70$ °C powder, but the amorphous

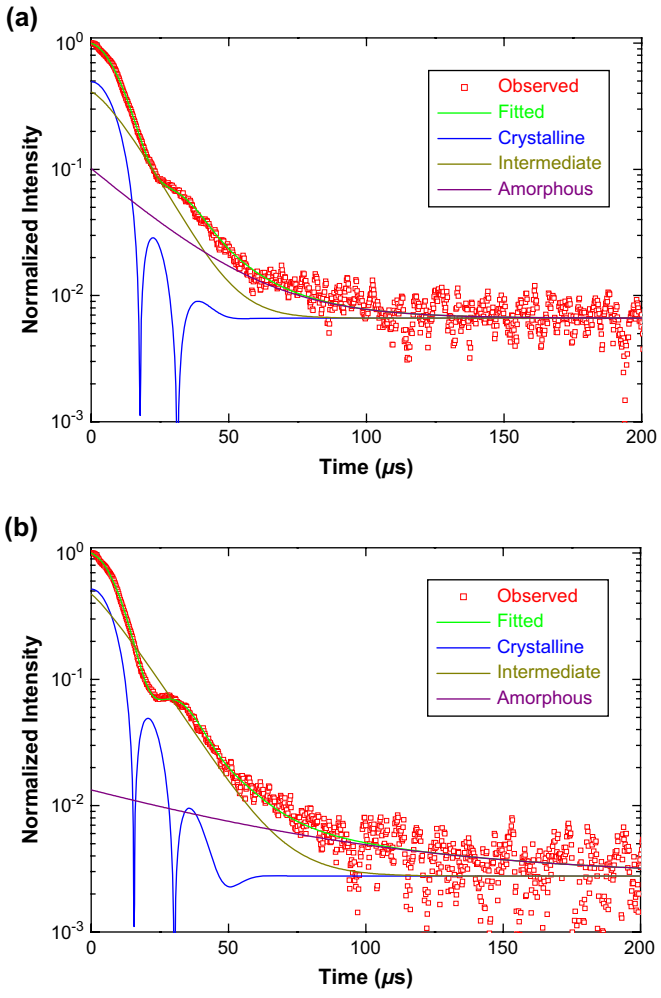

Fig. 7. Three-component resolutions of ^{1}H NMR FID profiles for the $T_{poly} = 20$ °C (a) and 70 °C powders (b).

Table 1
Summarized spin-spin relaxation times T_2, calculated as the inverse of the integral width, for the different components resolved from ^{1}H NMR FID observed at room temperature for the original powders prepared at $T_{poly} = 20$ °C and 70 °C

T_{poly} (°C)	Crystalline (μs)	Intermediate (μs)	Amorphous (μs)
20	17.2	30.8	45.3
70	15.5	31.2	125

phase is more rigid for the $T_{poly} = 20$ °C powder. The detailed assignments of these different T_2 values are discussed later.

3.4. Changes in molecular motions during heating

These ^{1}H NMR relaxation behaviors change gradually with heating, similar to the TEM and WAXD results discussed earlier. Fig. 8 compares the FID profiles recorded during heating for the $T_{poly} = 20$ °C and the $T_{poly} = 70$ °C powders. The FID profiles of both reactor powders exhibit gentler slopes with increasing temperature, suggesting enhanced molecular motion. Three-component resolution using a universal Weibull/Sine function was performed for these series of FID profiles. The obtained results are summarized in Fig. 9, where each molecular motion is represented by the original value of the integral width. The highest value was obtained for the crystalline phase, and the lowest value for the amorphous phase. The middle value corresponds to the intermediate phase. Crystallinity was also calculated as the integral intensity for the crystalline phase as a percentage of the sum of the whole. During an early stage of heating, crystallinity decreases and exhibits a minimum value around 60 °C, then increases again for both powders. These decreases and subsequent increases in crystallinity coincide with those of the reflection intensities observed for WAXD profile changes during heating in this temperature range. However, the critical temperature at which the minimum crystallinity was obtained was different for these analytical techniques. This is attributed to the analytical basis of each technique. The NMR measurements using the solid-echo method detect ^{1}H spin-spin relaxation, which concerns with the smaller spatial size on the atomic scale. In contrast, WAXD measurements focus on the density periodicities within the crystalline domains on the nanometer scale. The larger size of the spatial targets for WAXD measurements causes the detection delay of the transition of the crystalline domains.

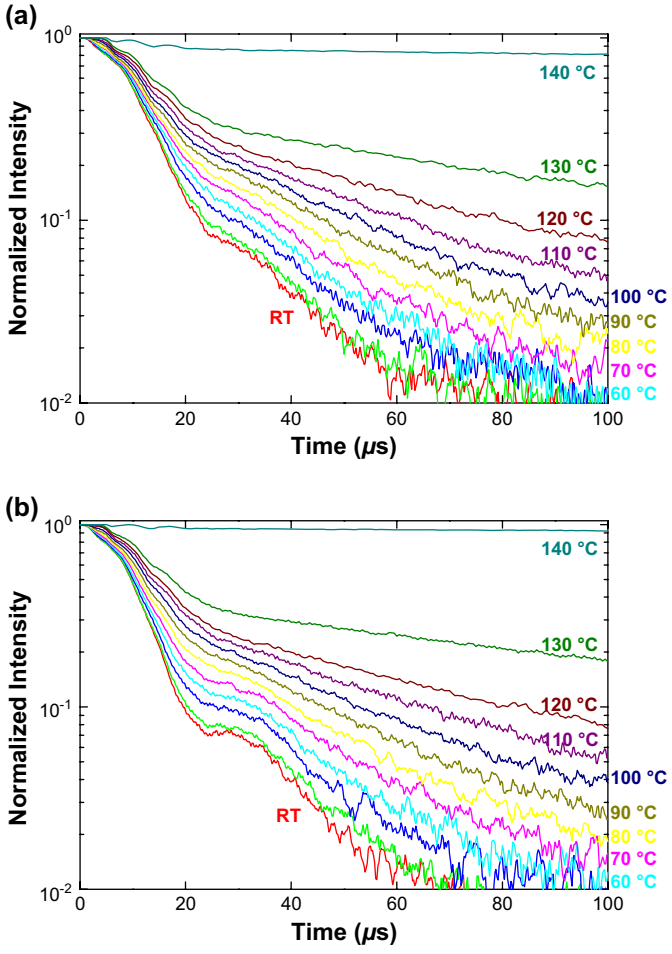

Fig. 8. Changes in the ^{1}H NMR FIDs during heating for the $T_{poly} = 20$ °C (a) and 70 °C powders (b).

Further heating produces maximum crystallinity at 120 °C for the $T_{poly} = 20$ °C powder and at 110 °C for the $T_{poly} = 70$ °C powder in Fig. 9. The abrupt drops in crystallinities beyond these temperatures are attributed to the sample melting. These temperatures exhibiting the maximum crystallinities coincide well with the temperatures at which the lamellae appear in the series of TEM observations presented above. These results indicate that the lamellar formation originates from melt-recrystallization on annealing and subsequent cooling.

The integral widths of the three different phases also change with increasing temperature for both powders. The trend of the intermediate phase is quite consistent, independent of the preparation T_{poly}. In contrast, the integral widths of the other two phases, i.e. crystalline and amorphous, exhibit remarkable differences within the entire temperature range, depending on T_{poly}. Fig. 10 compares the integral width changes during heating for each phase. There are only negligible difference between the $T_{poly} = 20$ °C powder and the $T_{poly} = 70$ °C powder above 90 °C in the crystalline phase, but the value is always lower in the $T_{poly} = 20$ °C powder below this temperature. Our recent solid-state NMR results [13] indicated that the larger crystallite size gives the higher integral width for the UHMW-PE samples prepared under different crystallization conditions. In this study, the smaller crystallite size of the monoclinic crystals within the $T_{poly} = 20$ °C powder is attributed to the lower integral width value. This difference in the integral width of the crystalline phase continues from room temperature to 60 °C. However, both powders exhibit similar crystalline widths above 90 °C because the aggregation of the crystalline domains into the larger size is completed at the higher temperature with crystal/crystal transition from the monoclinic to the orthorhombic forms, as indicated by TEM and WAXD results.

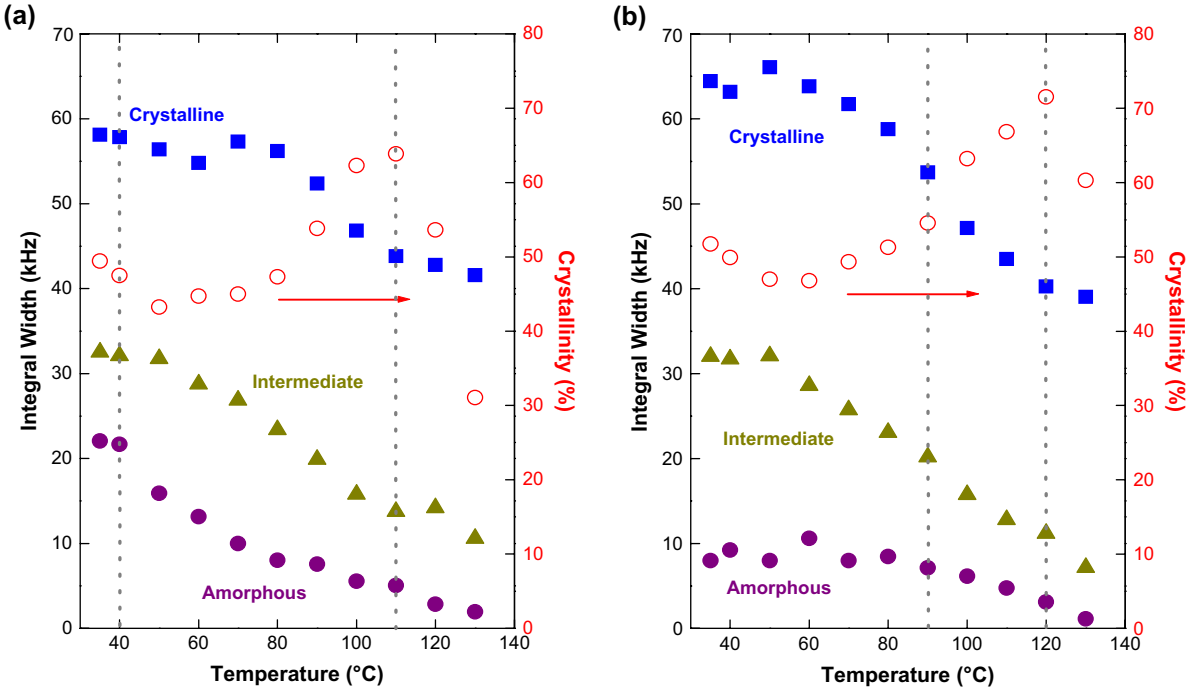

Fig. 9. Temperature dependencies of integral widths and crystallinity during heating for the $T_{poly} = 20$ °C (a) and 70 °C powders (b). Changes in the crystalline, intermediate and amorphous relaxations were plotted for each sample. The crystallinity was calculated as the component percentage of the crystalline component.

In contrast, the integral width of the amorphous phase is always larger for the $T_{poly} = 20$ °C powder than for the $T_{poly} = 70$ °C powder below 90 °C. This means that the molecular mobility of the $T_{poly} = 20$ °C powder is lower, due to the more restricted progress of the structural formation at the lower T_{poly}, as discussed above. It should be noted that the integral width of the $T_{poly} = 70$ °C powder coincides with that of the conventional melt-recrystallized PE [13], indicating the so-called randomly coiled state of the amorphous chains. Additionally, the amorphous width in the $T_{poly} = 70$ °C powder is constant below 90 °C. However, that of the $T_{poly} = 20$ °C powder begins to decrease at 40 °C, and finally duplicates those of the $T_{poly} = 70$ °C powder above 90 °C. The critical temperature at which the aggregation of the crystalline domains is evident in the TEM observations is 40 °C for the $T_{poly} = 20$ °C powder (Fig. 3). This synchronization of the morphological and molecular mobility changes suggests that the spatial motion of the amorphous chains induces an increase in the size of the crystalline domains during annealing. In contrast, the corresponding changes for the $T_{poly} = 70$ °C powder occur at 90 °C. Similar coincidence of the critical temperatures for the morphological and molecular mobility changes for both reactor powders supports the above assignment of the phase development mechanism during annealing. The constrained molecular motion of as-polymerized amorphous chains surrounding the crystalline domains is released when the annealing reaches the critical temperature, which always exceeds the maximum temperature experienced during polymerization. This molecular motion of the amorphous phases unlocks the crystalline domains so they can be aggregated into the larger spatial area.

3.5. Structural development mechanism of reactor powder

The structural development model in Fig. 11 is a combination of all the information obtained from TEM observation, WAXD and NMR measurements. The results of the morphological changes during annealing demonstrate that the actual polymerization commenced when the temperature was 20 °C higher than the preparation T_{poly} for each of the reactor powders. This slight temperature difference corresponds to an exothermic reaction near the active sites on the catalyst, where continuous chain growth occurs. Rapid crystallization occurs for the lower T_{poly} as soon as the shorter chains are produced at the active sites, and the resultant crystalline domains retain the constraints of the molecular chains. Therefore, the crystalline phase of the lower T_{poly} powder contains a larger amount of the monoclinic form within a smaller domain. The molecular mobility of the amorphous phase is also restricted in the reactor powder prepared at the lower T_{poly}. In contrast, the higher T_{poly} generates the stepwise processes of the initial chain growth and subsequent crystallization of the grown chains. Therefore, larger crystalline domains with the usual orthorhombic form are produced with a less-constrained amorphous phase. After these reactor powders are annealed beyond the temperature experienced during polymerization near the active site, the amorphous chains surrounding the crystalline domains become mobile. This amorphous chain motion characteristically unlocks and induces the aggregation of the crystalline domains by releasing the lattice constraint. These phase changes in the crystalline and amorphous phases are synchronized through the intermediate phase that connects

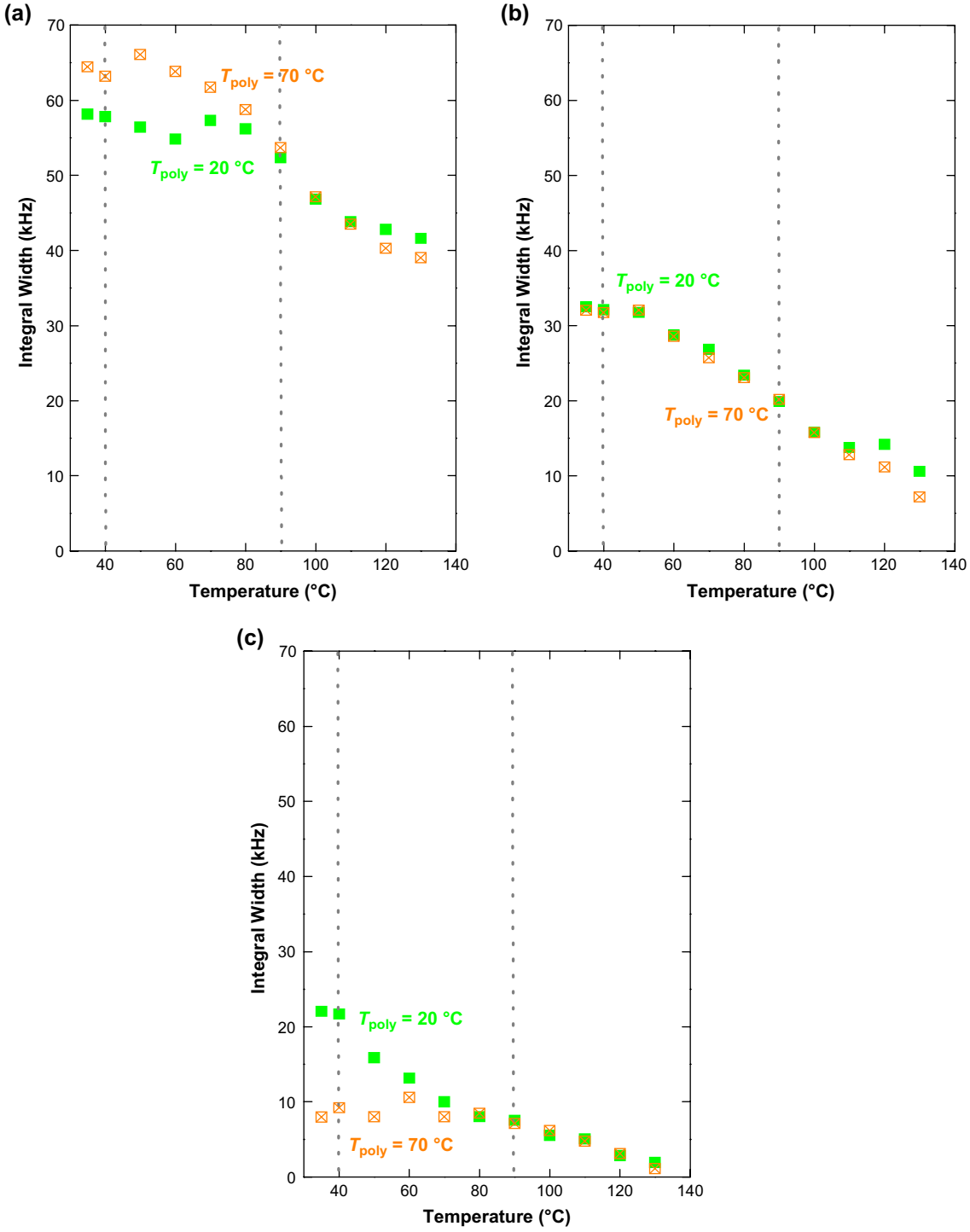

Fig. 10. Summarized changes in the integral width during heating of $T_{poly} = 20$ °C and 70 °C powders. The results of (a) crystalline, (b) intermediate and (c) amorphous components obtained in Fig. 9 are compared.

them. Thus, the molecular motion of the intermediate phase exhibits a gradual change during heating for both reactor powders. Further annealing gives the partial melting, as confirmed by the reduction of crystallinity, and destroys such domain-aggregate structure. However, cooling after annealing induces the usual lamellar crystallization, which is recognizable in the resultant powder morphology.

4. Conclusions

This study investigated the structural changes during annealing of PE reactor powders prepared under different T_{poly}s using a combination of TEM observation, WAXD and ^{1}H NMR measurements. TEM results suggest that the reactor powder morphology is composed of unique crystalline

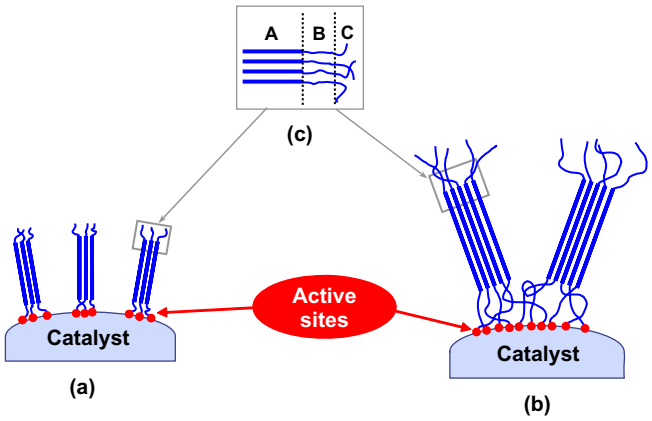

Fig. 11. Structural development model during polymerization including chain growth and crystallization at $T_{poly} = 20\,^{\circ}C$ (a) and $70\,^{\circ}C$ (b). Panel (c) indicates the intermediate region B sandwiched between crystalline A and amorphous C phases.

domains that are formed during polymerization. Beyond each critical temperature, corresponding to 20 °C higher than that of the preparation T_{poly}, the crystalline domains begin to aggregate for both reactor powders. These results mean that the critical temperatures are the maximum temperatures experienced during polymerization near the active sites on the catalyst, where both chain growth and crystallization proceed. NMR results indicated that the enhancement of the amorphous chains induces the above-mentioned morphological changes in PE reactor powders. WAXD results demonstrated that the lower T_{poly} powder contains a larger amount of the monoclinic crystals within the smaller size. A similar restriction of the molecular mobility was also detected for the amorphous phase of the lower T_{poly} powder. These results imply that phase development during polymerization of the lower T_{poly} proceeds with the constraint state. At the lower T_{poly}, rapid crystallization is repeated one after another even when the shorter chain segments grow at the active sites, meaning that the rate-determining step of the phase development is the chain growth during polymerization. In contrast, the crystallization after the longer chains grow is expected at the higher T_{poly}, meaning that the crystallization is the rate-determining step in this case. This competitive mechanism composed of the chain growth and crystallization is thought to be the cause of the characteristic reactor powder morphologies, depending on the preparation T_{poly}.

Acknowledgements

Synchrotron WAXD measurements were performed under approval of the Photon Factory Program Advisory Committee (Proposal 2004G265). This work was partly supported by the Industrial Technology Research Grant Program in '04 from the New Energy and Industrial Technology Development Organization (NEDO) of Japan and The Eno Science Foundation.

References

[1] Blais P, Manley RStJ. J Polym Sci Part A-1 1968;6:291.
[2] Keller A, Willmouth FM. Macromol Chem 1969;121:42.
[3] Graff RJL, Kortleve G, Vonk CG. J Polym Sci Polym Lett 1970;8:735.
[4] Chanzy HD, Revol JF, Marchessault RH, Lamandé A. Kolloid Z Z Polym 1973;251:563.
[5] Moñoz-Escalona A, Parada A. J Cryst Growth 1980;48:250.
[6] Kakugo M, Sadatoshi H, Yokoyama M. J Polym Sci Polym Lett 1986;24:171.
[7] Smith P, Chanzy HD, Rotzinger BP. J Mater Sci 1987;22:523.
[8] Kakugo M, Sadatoshi H, Yokoyama M, Kojima K. Macromolecules 1989;22:547.
[9] Kakugo M, Sadatoshi H, Sakai J, Yokoyama M. Macromolecules 1989;22:3172.
[10] Tervoort-Engelen YMT, Lemstra PJ. Polym Commun 1991;32:343.
[11] Nooijen GAH. Eur Polym J 1994;30:11.
[12] Uehara H, Nakae M, Kanamoto T, Ohtsu O, Sano A, Matsuura K. Polymer 1998;39:6127.
[13] Uehara H, Yamanobe T, Komoto T. Macromolecules 2000;33:4861.
[14] Lin CH, Sheu CY. Macromol Rapid Commun 2000;21:1058.
[15] Ivan'kova EM, Myasnikova LP, Marikhin VA, Baulin AA, Volchek BZ. J Macromol Sci Phys 2001;40:813.
[16] Uehara H, Aoike T, Yamanobe T, Komoto T. Macromolecules 2002;35:2640.
[17] Tsobkallo K, Vasilieva V, Khizhnyak S, Pakhomov P, Galitsyn V, Ruhl E, et al. Polymer 2003;44:1613.
[18] Tsobkallo K, Vasilieva V, Kakiage M, Uehara H, Tshmel A. J Macromol Sci Phys 2006;45:407.
[19] Uehara H, Yoshida R, Kakiage M, Yamanobe T, Komoto T. Ind Eng Chem Res 2006;45:7801.
[20] Hearle JWS. High-performance fibers. Cambridge: CRC Press; 2001.
[21] Kanamoto T, Ohama T, Tanaka K, Takeda M, Porter RS. Polymer 1987;28:1517.
[22] Rotzinger BP, Chanzy HD, Smith P. Polymer 1989;30:1814.
[23] Wang LH, Ottani S, Porter RS. Polymer 1991;32:1776.
[24] Porter RS, Kanamoto T, Zachariades AE. Polymer 1994;35:4979.
[25] Uehara H, Kanamoto T, Kawaguchi A, Murakami S. Macromolecules 1996;29:1540.
[26] Uehara H, Hirao T, Yamanobe T, Komoto T, Yamamoto Y. Polymer 2006;47:7145.
[27] Uehara H, Jounai K, Endo R, Okuyama H, Kanamoto T, Porter RS. Polym J 1997;29:198.
[28] Endo R, Jounai K, Uehara H, Kanamoto T, Porter RS. J Polym Sci Polym Phys Ed 1998;36:2551.
[29] Klüver W, Ruland W. Prog Colloid Polym Sci 1978;64:255.
[30] Voigt G, Kimmich R. Polymer 1980;21:1001.
[31] Kamel I, Charlesby A. J Polym Sci Polym Phys Ed 1981;19:803.
[32] Bergmann K, Schmiedberger H, Unterforsthuber K. Colloid Polym Sci 1984;262:283.
[33] Dadayli D, Harris RK, Kenwright AM, Say BJ, Sunnetcioglu MM. Polymer 1994;35:4083.
[34] Chen W, Fu Y, Wunderlich B, Cheng J. J Polym Sci Polym Phys Ed 1994;32:2661.
[35] Cheng J, Fone M, Reddy VN, Schwartz KB, Fisher HP, Wunderlich B. J Polym Sci Polym Phys Ed 1994;32:2683.
[36] Fu Y, Chen W, Pyde M, Londono D, Annis B, Boller A, et al. J Macromol Sci Phys 1996;B35:37.
[37] Kuwabara K, Kaji H, Horii F, Bassett DC, Olley RH. Macromolecules 1997;30:7516.
[38] Hansen EW, Kristiansen PE, Pedersen B. J Phys Chem B 1998; 102:5444.
[39] Kristiansen PE, Hansen EW, Pedersen B. J Phys Chem B 1999; 103:3552.
[40] Kristiansen PE, Hansen EW, Perdersen B. Polymer 2000;41:311.
[41] de Langen M, Luigjes H, Prons KO. Polymer 2000;41:1183.
[42] Hu WG, Schmidt-Rohr K. Polymer 2000;41:2979.

[43] Kristiansen PE, Hansen EW, Pedersen B. Polymer 2001;42:1969.
[44] Leisen J, Beckham HW, Sharaf MA. Macromolecules 2004;37:8028.
[45] Maus A, Hertlein C, Saalwächter K. Macromol Chem Phys 2006;207:1150.
[46] Klug HP, Alexander LE. X-ray diffraction procedures. New York: John Wiley & Sons; 1974.
[47] Miyaji H, Asahi T, Miyamoto Y, Asai K. J Polym Sci Polym Phys Ed 1987;25:159.
[48] Ottani S, Wagner BE, Porter RS. Polym Commun 1990;31:370.
[49] Kawaguchi A, Murakami S, Katayama K, Mihoichi M, Ohta T. Bull Inst Chem Kyoto Univ 1991;69:145.
[50] Abragam A. Principles of nuclear magnetism. Oxford: Clarendon; 1961.
[51] Brereton MG. J Chem Phys 1991;94:2136.